

Precise measurement of the mass difference and the binding energy of hypertriton and antihypertriton

The STAR Collaboration

Using the STAR (Solenoidal Tracker At RHIC) detector^{1–3} at the Relativistic Heavy Ion Collider (RHIC), we have measured the Λ hyperon binding energy B_Λ for the hypertriton, which is the lightest hypernucleus yet discovered and consists of a proton, a neutron, and a Λ hyperon. The measured B_Λ differs from the widely used value^{4,5} and from predictions in which the hypertriton is modeled as a Λ weakly bound to a deuterium nucleus^{6–9}. Our results place stringent constraints on the hyperon-nucleon interaction^{10,11}, and provide critical inputs for studying neutron star interiors, where strange matter may be present¹². The same data also permit more precise comparison between the masses of the hypertriton and the antihypertriton. Matter-antimatter symmetry¹³ pertaining to the binding of strange and antistrange quarks (s and \bar{s}) in a nucleus is thus tested quantitatively for the first time. No deviation from the expected exact symmetry is observed.

The CPT theorem^{14–17} holds that all processes must exactly conserve the combined operation of C (charge conjugation, which interchanges a particle with its antiparticle), P (parity, which reverses the direction of all spatial axes), and T (time reversal). One implication is that every particle should have a mass and lifetime identical to those of its antiparticle, but opposite electric charge and magnetic moment¹³. No CPT violation has ever been observed^{13,18,19}. Qualitatively different tests of CPT symmetry are a continuing priority for fundamental physics, as are revisitations of past tests with improved accuracy. While CPT invariance has been verified to a precision of 10^{-19} in the strange quark sector for kaons¹⁸, we present here the first test of CPT in a nucleus having strangeness content.

Hypernuclei are natural hyperon-baryon correlation systems, and thus provide direct access to the hyperon-nucleon (YN) interaction through measurements of the binding energy B_Λ in a hypernucleus^{20,21}. However, in a half-century of research, the creation of the hypertriton and precise measurements of its properties have proven difficult in contrast to the study of heavier hypernuclei that are produced via the traditional method of a kaon beam incident on a nuclear target²². Early measurements of the hypertriton B_Λ are consistent with zero and span a wide range characterised by a full width at half maximum of 2.1 MeV^{4,5,23}. Modern facilities now permit an improved understanding of the YN interaction via more precise measurements of hyperon binding in hypernuclei, such as the lifetime measurement for the hypertriton²⁴. Progress in understanding the YN interaction and the equation of state of hypernuclear matter has astrophysical implications in the understanding of neutron star properties. Inclusion of hyperons in the cores of neutron stars softens the equation of state, and thus reduces the stellar masses^{12,22,25}. In model calculations, the maximum mass of the neutron star can vary from 0.4 to 2.4 of solar masses, depending on the strength of the ΛNN three-body repulsive potential which is directly related to the Λ binding energy in hypernuclei^{25,26}.

Nuclear collisions at ultrarelativistic energies, such as those studied at RHIC, create a hot and dense phase of matter containing approximately equal numbers of quarks and antiquarks. In this phase, called the quark-gluon plasma²⁷ (QGP), quarks are free to move throughout the volume of the nuclear collision region. The QGP exhibits fluid properties with an exceptionally low ratio of viscosity to entropy density²⁸, and a far higher vorticity than any other system produced in a laboratory or observed in nature²⁹. The QGP persists for only a few times 10^{-23} seconds, then cools and transitions into a lower temperature phase comprised of mesons, baryons and antibaryons, including the occasional antinucleus or antihypernucleus^{9,11}. Thus these collisions offer an ideal laboratory to explore fundamental physics involving nuclei, hypernuclei, and their antimatter partners.

In this letter, we present two measurements from gold-gold collisions at a center-of-mass energy per nucleon pair of $\sqrt{s_{NN}} = 200$ GeV: the relative mass difference between ${}^3_\Lambda H$ (the hypertriton) and ${}^3_{\bar{\Lambda}} \bar{H}$ (the antihypertriton), as well as the Λ hyperon binding energy for ${}^3_\Lambda H$ and ${}^3_{\bar{\Lambda}} \bar{H}$. The Λ hyperon binding energy of ${}^3_\Lambda H$ is defined as $B_\Lambda = (m_d + m_\Lambda - m_{{}^3_\Lambda H})c^2$, where m_d , m_Λ , $m_{{}^3_\Lambda H}$ are the deuteron mass taken from the CODATA³⁰, the Λ hyperon mass taken from the PDG¹⁸, and the ${}^3_\Lambda H$ mass reported in this letter, and where c is the speed of light. The main detectors used in this analysis are the STAR Time Projection Chamber (TPC)¹ and the Heavy Flavor Tracker (HFT)² for high-precision tracking, and the TPC and the Time Of Flight detector (TOF)³ for charged particle identification. The TPC is immersed in a solenoidal magnetic field of 0.5 T parallel to the beam direction, and is used in conjunction with the HFT for charged particle tracking in three dimensions. The HFT includes three subsystems: Pixel (PXL), which consists of two cylindrical layers at radii 2.8 and 8 cm from the beam, the Intermediate Silicon Tracker (IST) at a radius of 14 cm, and the Silicon Strip Detector (SSD) at a radius of 22 cm. The spatial resolution of the HFT² is better than $30 \mu\text{m}$ for tracks with a momentum of 1 GeV/c. The mean energy loss per unit track length ($\langle dE/dx \rangle$) in the TPC gas and the speed (β) determined from TOF measurements are used to identify particles. The $\langle dE/dx \rangle$ resolution¹ is 7.5% and the TOF timing resolution³ is 95 ps.

The hypernucleus ${}^3_\Lambda H$ is reconstructed through its mesonic decay channels ${}^3_\Lambda H \rightarrow {}^3\text{He} + \pi^-$ (2-body decay) and

${}^3_{\Lambda}\text{H} \rightarrow d + p + \pi^-$ (3-body decay). Fig. 1 depicts a typical event in which a ${}^3_{\Lambda}\bar{\text{H}}$ candidate decays to $\bar{d} + \bar{p} + \pi^+$ in the STAR HFT and TPC. The ${}^3_{\Lambda}\bar{\text{H}}$ candidate is produced at the primary vertex of a gold-gold collision and remains in flight for a distance on the order of centimeters, as shown by the dashed green curve starting at the center of the right-hand side of the figure, before decaying as depicted by the bold coloured curves.

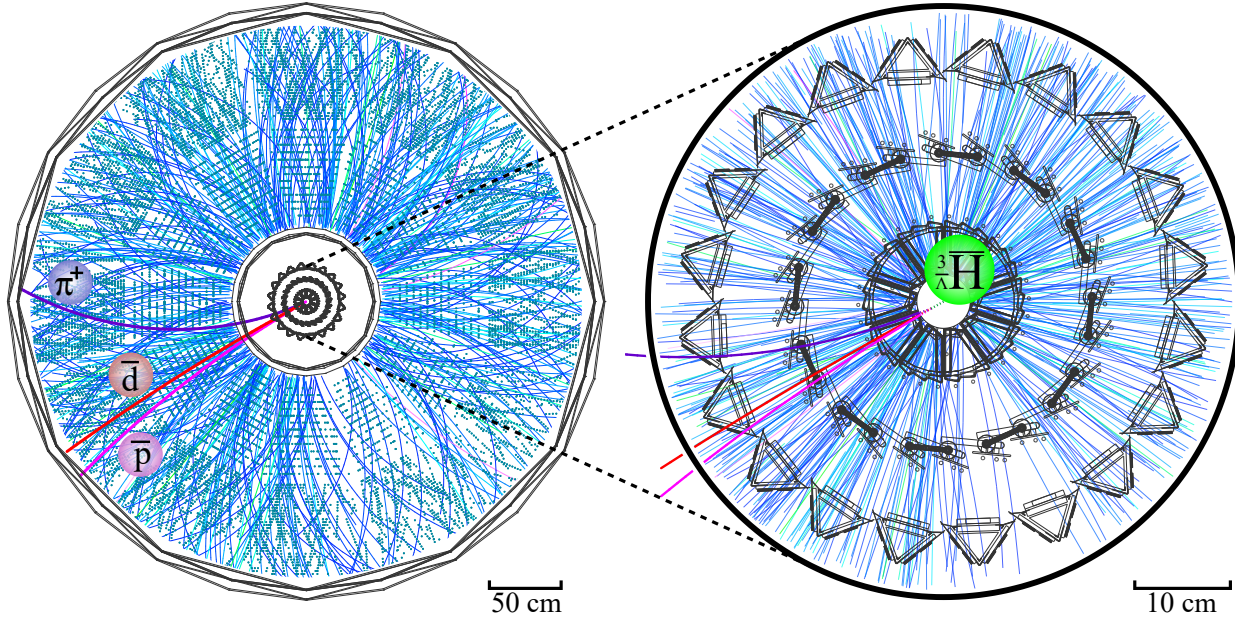


Figure 1 | A typical event in which there is a candidate for the production and 3-body decay of ${}^3_{\Lambda}\bar{\text{H}}$ in the STAR HFT and TPC detectors. The left side shows a less magnified view of the STAR detector with the beam axis normal to the page, including a projected view of the large number of tracks detected by the TPC in a typical gold-gold collision. The right side shows an end-on view of the four cylindrical layers of the HFT located at the center of the TPC. The bold red, pink, and violet curves represent the trajectories of the \bar{d} , \bar{p} and π^+ decay daughters, respectively. The reconstructed decay daughters can be traced back to the decay vertex, at where the ${}^3_{\Lambda}\bar{\text{H}}$ decays after flying for a distance on the order of centimeters, as shown by the dashed green curve starting at the center of the right side.

Comparisons of the measured $\langle dE/dx \rangle$ and β values for each track with their expected values under different mass hypotheses allow decay daughters to be identified. Panel a of Fig. 2 presents $\langle dE/dx \rangle$ versus rigidity (p/q , where p is the momentum and q is the electric charge in units of the elementary charge e), while panel b shows $1/\beta$ versus rigidity. It can be seen that the decay daughter species for ${}^3_{\Lambda}\text{H}$ and ${}^3_{\Lambda}\bar{\text{H}}$ are cleanly identified over a wide rigidity range. The helical trajectories of the decay daughter particles can be followed back in time to each secondary decay vertex and used to reconstruct the decay topology of the parent (anti)hypernucleus. The effects of energy loss (ranging from about 0.2% for π^\pm to about 3% for ${}^3\text{He}$) and TPC field distortion on the measured momenta of the decay daughters are corrected for by data-driven calibration using the world-average Λ mass compiled by the PDG¹⁸. Due to the high-precision tracking and particle identification capabilities of the STAR experiment, the invariant mass ($\sqrt{(\sum E_i)^2 - (\sum \vec{p}_i)^2}$, where E_i is the energy and \vec{p}_i the momentum of the i th decay daughter) of each parent is reconstructed with a low level of background as shown in panels c and d of Fig. 2. The background originates from combinatorial contamination and particle misidentification. The significance $S/\sqrt{S+B}$, where S is signal counts ($158 {}^3_{\Lambda}\text{H}$ and $62 {}^3_{\Lambda}\bar{\text{H}}$ candidates) and B is background in the invariant mass window of $2.986 - 2.996 \text{ GeV}/c^2$, is 11.5 for ${}^3_{\Lambda}\text{H}$ and 6.9 for ${}^3_{\Lambda}\bar{\text{H}}$. The signal-to-background ratio is close to a factor of 23 better than an earlier measurement from the same experiment using only the TPC²⁴.

The (anti)hypernucleus invariant mass distributions reconstructed through 2-body and 3-body decay channels are each fitted with a Gaussian function plus a straight line, using the unbinned maximum likelihood method. The mass parameters are extracted from the peak positions of the invariant mass distributions. The final results are obtained as the average of the mass values from the 2-body and 3-body decay channels weighted by the reciprocal of the squared statistical uncertainties. The main systematic uncertainty arises from the imperfections in the energy loss and field distortion corrections applied to the tracking of the decay daughters, which is estimated to be $0.11 \text{ MeV}/c^2$ (37 ppm). Other sources of systematic uncertainties, including those from event selection, track quality cuts, decay topology cuts and fit procedure, are found to have a negligible impact on the final results. Accordingly, the measured masses are

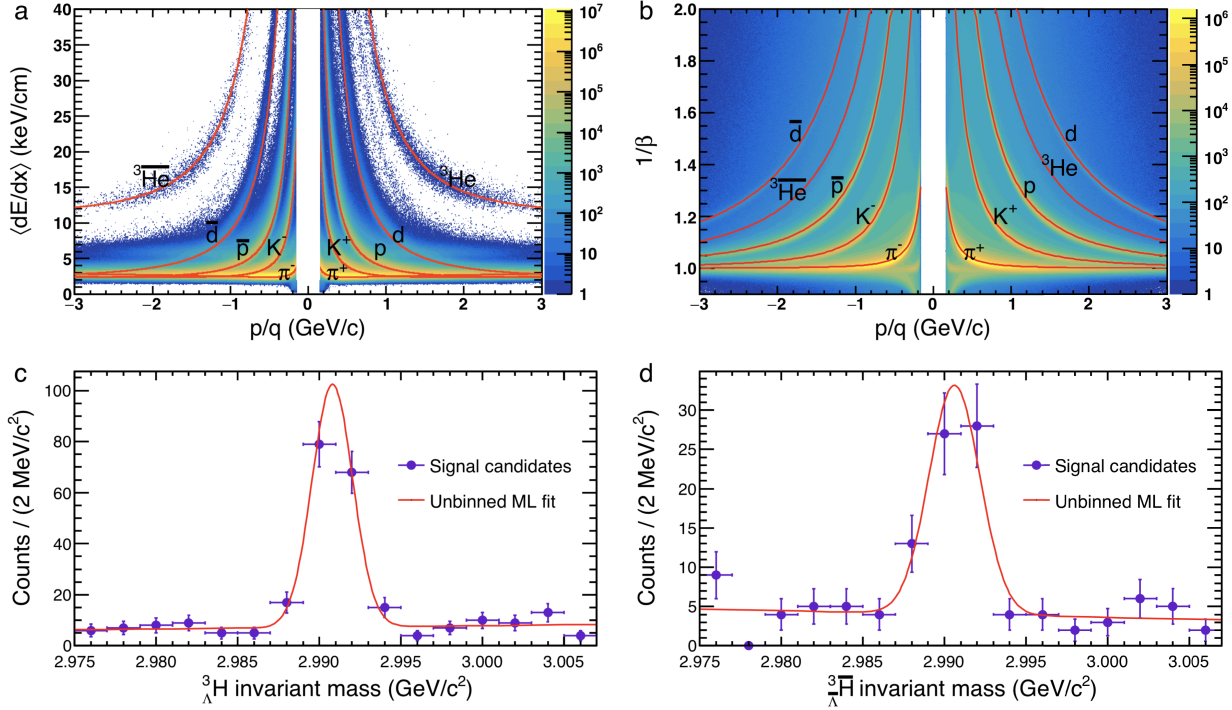


Figure 2 | Particle identification using TPC and TOF, and the invariant mass distributions for ${}^3\Lambda H$ and ${}^3\bar{\Lambda} H$ reconstruction. $\langle dE/dx \rangle$ versus p/q is presented in panel a, and $1/\beta$ versus p/q in panel b. In both cases, the colored bands show the measured data for each species of charged particle, while the red curves show the expected values. Charged particles are identified by comparing the observed $\langle dE/dx \rangle$ and $1/\beta$ with the expected values. The invariant mass distributions of ${}^3\Lambda H$ and ${}^3\bar{\Lambda} H$, which are reconstructed through 2-body and 3-body decay channels, are shown as data points with statistical error bars only in panels c and d, respectively. The red curves represent a fit with a Gaussian function plus a linear background, using the unbinned Maximum Likelihood (ML) method. The ${}^3\Lambda H$ and ${}^3\bar{\Lambda} H$ mass determination is not based on these curves; see the text for details.

$$m_{{}^3\Lambda H} = 2990.95 \pm 0.13(\text{stat.}) \pm 0.11(\text{syst.}) \text{ MeV}/c^2$$

$$m_{{}^3\bar{\Lambda} H} = 2990.60 \pm 0.28(\text{stat.}) \pm 0.11(\text{syst.}) \text{ MeV}/c^2$$

The average mass (weighted by the reciprocal of squared statistical uncertainties) for ${}^3\Lambda H$ and ${}^3\bar{\Lambda} H$ combined is

$$m = 2990.89 \pm 0.12(\text{stat.}) \pm 0.11(\text{syst.}) \text{ MeV}/c^2 \quad (1)$$

The relative mass difference between ${}^3\Lambda H$ and ${}^3\bar{\Lambda} H$ is

$$\frac{\Delta m}{m} = \frac{m_{{}^3\Lambda H} - m_{{}^3\bar{\Lambda} H}}{m} = [1.1 \pm 1.0(\text{stat.}) \pm 0.5(\text{syst.})] \times 10^{-4}$$

which is displayed in Fig. 3 along with the relative mass-to-charge ratio differences between d and \bar{d} and between ${}^3\text{He}$ and ${}^3\bar{\text{He}}$ measured by the ALICE Collaboration¹⁹. The mass difference between ${}^3\Lambda H$ and ${}^3\bar{\Lambda} H$ observed in the present data is consistent with zero. The current measurement extends the validation of CPT invariance with high precision to a nucleus containing a strange quark.

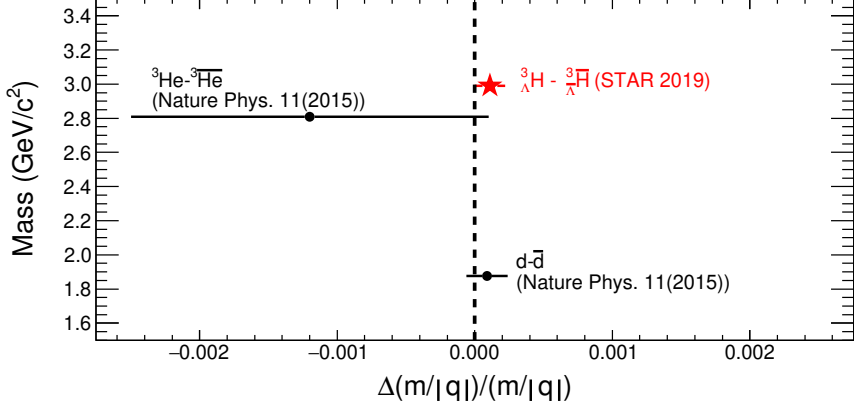


Figure 3 | Measurements of the relative mass-to-charge ratio differences between nuclei and antinuclei. The current STAR measurement of the relative mass difference $\Delta m/m$ between ${}^3\Lambda H$ and ${}^3\bar{\Lambda}H$ is shown by the red star marker. The differences between d and \bar{d} and between 3He and ${}^3\bar{He}$ measured by the ALICE Collaboration¹⁹ are also shown here. The dotted vertical line at zero on the horizontal axis is the expectation from CPT invariance. The horizontal error bars represent the sum in quadrature of the statistical and systematic uncertainties.

The Λ binding energy B_Λ for ${}^3\Lambda H$ and ${}^3\bar{\Lambda}H$ is calculated using the mass measurement shown in equation (1). We obtain

$$B_\Lambda = 0.41 \pm 0.12(\text{stat.}) \pm 0.11(\text{syst.}) \text{ MeV}$$

This binding energy is presented in Fig. 4 (left panel) along with earlier measurements^{4,31–33} from nuclear emulsion and helium bubble chamber experiments. The current STAR result differs from zero with a significance of 2.6σ . The masses used for Λ , π^- , p , d and 3He in the early measurements of B_Λ were different from contemporary standard CODATA³⁰ and PDG¹⁸ values. Thus the early B_Λ values have been recalculated using the most precise mass values known today, and the recalibrated results are shown by short horizontal magenta lines in Fig. 4 (left panel; see Methods section for details). Even after recalibration, the central value of the current STAR measurement is larger than the measurement from 1973⁴ which is widely used. It has been pointed out in Ref.²³ that for measurements of B_Λ for p-shell hypernuclei, there exists a discrepancy in the range of 0.4 to 0.8 MeV between emulsion data and other modern measurements. Whether the effect would be similar in s-shell hypernuclei such as the hypertriton is unclear, but such a discrepancy is much larger than the systematic uncertainty assigned to emulsion measurements³⁴. Until this discrepancy is well understood, an average of the current measurement with early results can not be reliably carried out.

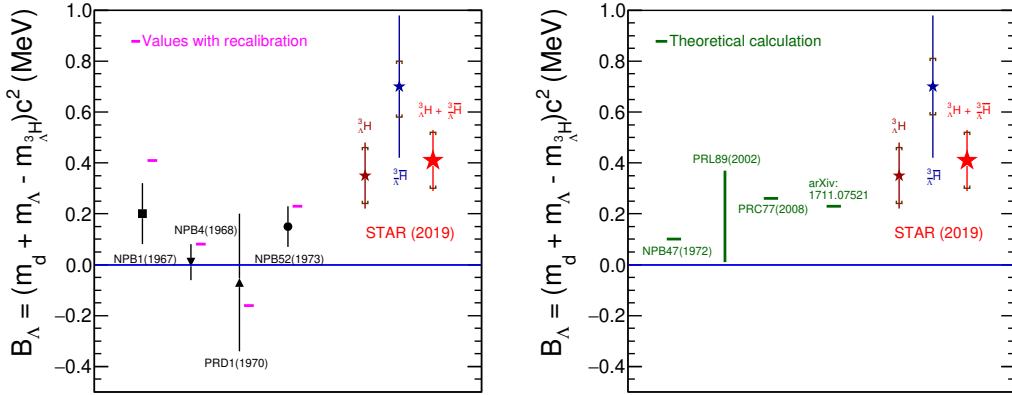


Figure 4 | Comparison of the STAR results with earlier measurements (left) and theoretical calculations (right) of B_Λ for ${}^3\Lambda H$ and ${}^3\bar{\Lambda}H$. The black points and their error bars (which are the reported statistical uncertainties) represent B_Λ for ${}^3\Lambda H$ based on earlier data^{4,31–33}. The short horizontal magenta lines represent the best estimates of B_Λ for ${}^3\Lambda H$ based on the same early data but using modern hadron and nucleus masses. The current STAR measurement plotted here is based on a combination of ${}^3\Lambda H$ and ${}^3\bar{\Lambda}H$ assuming CPT invariance. Error bars show statistical uncertainties and caps show systematic errors. The green lines in the right panel represent theoretical calculations of B_Λ .

In addition to measurements, theoretical calculations of B_Λ for ${}^3_\Lambda\text{H}$ are also available (see right panel of Fig. 4). For example, Dalitz calculated $B_\Lambda = 0.10$ MeV in 1972³⁵, while B_Λ values in the range 0.01-0.37 MeV were obtained through an *ab initio* calculation in 2002³⁶. More recent theoretical calculations have yielded larger B_Λ values. In 2008, $B_\Lambda = 0.262$ MeV was obtained through SU(6) quark model baryon-baryon interactions³⁷, and B_Λ was found to be 0.23 MeV using auxiliary field diffusion Monte Carlo (AFDMC) in 2018³⁸. The dispersion of the results from the different calculations emphasizes the need for a precise determination of B_Λ from experiments. In a related matter, the latest compilation of measurements yields a ${}^3_\Lambda\text{H}$ lifetime $(30 \pm 8)\%$ shorter than the free Λ lifetime³⁹. A calculation in which the closure approximation was introduced to evaluate the wavefunctions by solving the three-body Faddeev equations, also indicates that the ${}^3_\Lambda\text{H}$ lifetime is $(19 \pm 2)\%$ smaller than that of Λ ³⁹. The larger B_Λ value and shorter lifetime suggest a stronger YN interaction between the Λ and the nuclear core in ${}^3_\Lambda\text{H}$, which may require a re-evaluation of the inference that the ${}^3_\Lambda\text{H}$ can be regarded as a simple weakly-bound Λ -deuteron system.

In summary, we report the first test of CPT invariance in the sector of hypernuclear matter where (anti)strange quarks play a role in (anti)nuclear binding. The relative mass difference between the hypertriton and antihypertriton is $[1.1 \pm 1.0(\text{stat.}) \pm 0.5(\text{syst.})] \times 10^{-4}$, consistent with no violation of CPT symmetry. Prior comparisons of nuclear binding for nuclei and antinuclei involved only up and down quarks, and this measurement both includes a strange quark and improves the uncertainty for mass number $A = 3$ by roughly an order of magnitude. We also report a new measurement of the Λ hyperon binding energy in the hypertriton: $B_\Lambda = 0.41 \pm 0.12(\text{stat.}) \pm 0.11(\text{syst.})$ MeV. The value differs from zero with a significance of 2.6σ , and is larger than the prior measurement from 1973⁴ which is widely used. Models in which the hypertriton is treated as a weakly-bound Λ -deuteron system predict smaller B_Λ values. These results constrain the hyperon-nucleon interaction, providing improved data to understand the role of hyperons in neutron stars, and thus have wide-ranging implications spanning nuclear physics, particle physics, and astrophysics.

References

- [1] Anderson, M. *et al.* The STAR time projection chamber: a unique tool for studying high multiplicity events at RHIC. *Nucl. Inst. Methods Phys. Res. A* **499**, 659-678 (2003).
- [2] Contin, G. *et al.* The STAR MAPS-based PiXeL detector. *Nucl. Inst. Methods Phys. Res. A* **907**, 60-80 (2018).
- [3] Llope, W. J. (For the STAR Collaboration). Multigap RPCs in the STAR experiment at RHIC. *Nucl. Inst. Methods Phys. Res. A* **661**, S110-S113 (2012).
- [4] Juric, M. *et al.* A new determination of the binding-energy values of the light hypernuclei ($A \leq 15$). *Nucl. Phys. B* **52**, 1-30 (1973).
- [5] Dalitz, R. H. 50 years of hypernucleus physics. II. The later years. *Nucl. Phys. A* **754**, 14-24 (2005).
- [6] Rayet, M. & Dalitz, R. H. The lifetime of ${}^3\text{H}_\Lambda$. *Nuovo Cimento A* **46**, 786-794 (1966).
- [7] Kamada, H., Golak, J., Miyagawa, K., Witala, H. & Glöckle, W. π -mesonic decay of the hypertriton. *Phys. Rev. C* **57**, 1595-1603 (1998).
- [8] Hammer, H.-W. The hypertriton in effective field theory. *Nucl. Phys. A* **705**, 173-189 (2002).
- [9] Chen, J. H., Keane, D., Ma, Y. G., Tang, A. H. & Xu, Z. B. Antinuclei in heavy-ion collisions. *Phys. Rep.* **760**, 1-39 (2018).
- [10] Lattimer, J. M. & Prakash, M. The Physics of Neutron Stars. *Science* **304**, 536-542 (2004).
- [11] Abelev, B. I. *et al.* (STAR Collaboration). Observation of an Antimatter Hypernucleus. *Science* **328**, 58-62 (2010).
- [12] Chatterjee, D. & Vidaña, I. Do hyperons exist in the interior of neutron stars? *Eur. Phys. J. A* **52:29**, 1-18 (2016).
- [13] Costa, G. & Fogli, G. *Symmetries and Group Theory in Particle Physics: An Introduction to Space-time and Internal Symmetries*. (Springer-Verlag, Berlin, 2012).
- [14] Schwinger, J. The Theory of Quantized Fields. I. *Phys. Rev.* **82**, 914-927 (1951).
- [15] Lüders, G. Proof of the TCP Theorem. *Ann. Phys.* **2**, 1-15 (1957).

- [16] Pauli, W. *Niels Bohr And The Development Of Physics: Essays Dedicated To Niels Bohr On The Occasion Of His Seventieth Birthday*. (Pergamon Press, London, 1955).
- [17] Bell, J. S. Time Reversal in Field Theory. *Proc. Roy. Soc. Lond. A* **231**, 479-495 (1955).
- [18] Tanabashi, M. *et al.* (Particle Data Group). Review of particle physics. *Phys. Rev. D* **98**, 030001 (2018).
- [19] Adam, J. *et al.* (ALICE Collaboration). Precision measurement of the mass difference between light nuclei and anti-nuclei. *Nature Phys.* **11**, 811-814 (2015).
- [20] Contessi, L., Barnea, N. & Gal, A. Resolving the Λ hypernuclear overbinding problem in pionless effective field theory. *Phys. Rev. Lett.* **121**, 102502 (2018).
- [21] Beane, S. R. *et al.* (NPLQCD Collaboration). Light nuclei and hypernuclei from quantum chromodynamics in the limit of SU(3) flavor symmetry. *Phys. Rev. D* **87**, 034506 (2013).
- [22] Gal, A., Hungerford, E. V. & Millener, D. J. Strangeness in nuclear physics. *Rev. Mod. Phys.* **88**, 035004 (2016).
- [23] Achenbach, P., Bleser, S., Pochodzalla, J. & Steinen, M. High-precision measurement of the hypertriton mass. *PoS Hadron2017*, 207 (2018).
- [24] Adamczyk, L. *et al.* (STAR Collaboration). Measurement of the ${}^3_{\Lambda}\text{H}$ lifetime in Au+Au collisions at the BNL Relativistic Heavy Ion Collider. *Phys. Rev. C* **97**, 054909 (2018).
- [25] Lonardoni, D., Lovato, A., Gandolfi, S., & Pederiva, F. Hyperon Puzzle: Hints from Quantum Monte Carlo Calculations. *Phys. Rev. Lett.* **114**, 092301 (2015).
- [26] Fortin, M., Avancini, S. S., Providência, C. & Vidaña, I. Hypernuclei and massive neutron stars. *Phys. Rev. C* **95**, 065803 (2017).
- [27] Shuryak, E. V. Quantum chromodynamics and the theory of superdense matter. *Phys. Rep.* **61**, 71-158 (1980).
- [28] Braun-Munzinger, P., Koch, V., Schäfer, T. & Stachel, J. Properties of hot and dense matter from relativistic heavy ion collisions. *Phys. Rep.* **621**, 76-126 (2016).
- [29] Adamczyk, L. *et al.* (STAR collaboration). Global Λ hyperon polarization in nuclear collisions. *Nature* **548**, 62-65 (2017).
- [30] Mohr, P. J., Newell, D. B. & Taylor, B. N. CODATA recommended values of the fundamental physical constants: 2014. *Rev. Mod. Phys.* **88**, 035009 (2016).
- [31] Gajewski, W. *et al.* A compilation of binding energy values of light hypernuclei. *Nucl. Phys. B* **1**, 105-113 (1967).
- [32] Bohm, G. *et al.* A determination of the binding-energy values of light hypernuclei. *Nucl. Phys. B* **4**, 511-526 (1968).
- [33] Keyes, G. *et al.* Properties of ${}^3_{\Lambda}\text{H}$. *Phys. Rev. D* **1**, 66-77 (1970).
- [34] Davis, D. H. 50 years of hypernuclear physics I. The early experiments. *Nucl. Phys. A* **754**, 3-13 (2005).
- [35] Dalitz, R. H., Herndon, R. C. & Tang, Y. C. Phenomenological study of s-shell hypernuclei with ΛN and ΛNN potentials. *Nucl. Phys. B* **47**, 109-137 (1972).
- [36] Nemura, H., Akaishi, Y. & Suzuki, Y. Ab initio approach to s-shell hypernuclei ${}^3_{\Lambda}\text{H}$, ${}^4_{\Lambda}\text{H}$, ${}^4_{\Lambda}\text{He}$, and ${}^5_{\Lambda}\text{He}$ with a $\Lambda\text{N}-\Sigma\text{N}$ interaction. *Phys. Rev. Lett.* **89**, 142504 (2002).
- [37] Fujiwara, Y., Suzuki, Y., Kohno, M. & Miyagawa, K. Addendum to triton and hypertriton binding energies calculated from SU_6 quark-model baryon-baryon interactions. *Phys. Rev. C* **77**, 027001 (2008).
- [38] Lonardoni, D. & Pederiva, F. Medium-mass hypernuclei and the nucleon-isospin dependence of the three-body hyperon-nucleon-nucleon force. Preprint at <https://arxiv.org/abs/1711.07521> (2018).
- [39] Gal, A. & Garcilazo, H. Towards resolving the ${}^3_{\Lambda}\text{H}$ lifetime puzzle. *Phys. Lett. B* **791**, 48-53 (2019).

Acknowledgements

We thank the RHIC Operations Group and RCF at BNL, the NERSC Center at LBNL, and the Open Science Grid consortium for providing resources and support. This work was supported in part by the Office of Nuclear Physics within the U.S. DOE Office of Science, the U.S. National Science Foundation, the Ministry of Education and Science of the Russian Federation, National Natural Science Foundation of China, Chinese Academy of Science, the Ministry of Science and Technology of China and the Chinese Ministry of Education, the National Research Foundation of Korea, Czech Science Foundation and Ministry of Education, Youth and Sports of the Czech Republic, Hungarian National Research, Development and Innovation Office (FK-123824), New National Excellency Programme of the Hungarian Ministry of Human Capacities (UNKP-18-4), Department of Atomic Energy and Department of Science and Technology of the Government of India, the National Science Centre of Poland, the Ministry of Science, Education and Sports of the Republic of Croatia, RosAtom of Russia and German Bundesministerium fur Bildung, Wissenschaft, Forschung und Technologie (BMBF) and the Helmholtz Association.

Author contributions

All authors have made important contributions to this publication, in one or more of the areas of detector hardware and software, operation of the experiment and acquisition of data, and analysis of the results. All STAR collaboration members who are authors of this paper reviewed and approved the submitted manuscript.

STAR Collaboration

J. Adam¹², L. Adamczyk², J. R. Adams³⁵, J. K. Adkins²⁶, G. Agakishiev²⁴, M. M. Aggarwal³⁷, Z. Ahammed⁵⁷, I. Alekseev^{3,31}, D. M. Anderson⁵¹, R. Aoyama⁵⁴, A. Aparin²⁴, D. Arkhipkin⁵, E. C. Aschenauer⁵, M. U. Ashraf⁵³, F. Atetalla²⁵, A. Attri³⁷, G. S. Averichev²⁴, V. Bairathi³², K. Barish⁹, A. J. Bassill⁹, A. Behera⁴⁹, R. Bellwied¹⁹, A. Bhasin²³, A. K. Bhati³⁷, J. Bielcik¹³, J. Bielcikova³⁴, L. C. Bland⁵, I. G. Bordyuzhin³, J. D. Brandenburg^{5,46}, A. V. Brandin³¹, J. Bryslawskyj⁹, I. Bunzarov²⁴, J. Butterworth⁴², H. Caines⁶⁰, M. Calderón de la Barca Sánchez⁷, D. Cebra⁷, I. Chakaberia^{25,46}, P. Chaloupka¹³, B. K. Chan⁸, F-H. Chang³³, Z. Chang⁵, N. Chankova-Bunzarova²⁴, A. Chatterjee⁵⁷, S. Chattopadhyay⁵⁷, J. H. Chen⁴⁷, X. Chen⁴⁵, J. Cheng⁵³, M. Cherney¹², W. Christie⁵, H. J. Crawford⁶, M. Csand¹⁵, S. Das¹⁰, T. G. Dedovich²⁴, I. M. Deppner¹⁸, A. A. Derevschikov³⁹, L. Didenko⁵, C. Dilks³⁸, X. Dong²⁷, J. L. Drachenberg¹, J. C. Dunlop⁵, T. Edmonds⁴⁰, N. Elsey⁵⁹, J. Engelage⁶, G. Eppley⁴², R. Esha⁸, S. Esumi⁵⁴, O. Evdokimov¹¹, J. Ewigleben²⁸, O. Eyser⁵, R. Fatemi²⁶, S. Fazio⁵, P. Federic³⁴, J. Fedorisin²⁴, Y. Feng⁴⁰, P. Filip²⁴, E. Finch⁴⁸, Y. Fisyak⁵, L. Fulek², C. A. Gagliardi⁵¹, T. Galatyuk¹⁴, F. Geurts⁴², A. Gibson⁵⁶, D. Grosnick⁵⁶, A. Gupta²³, W. Guryn⁵, A. I. Hamad²⁵, A. Hamed⁵¹, J. W. Harris⁶⁰, L. He⁴⁰, S. Heppelmann⁷, S. Heppelmann³⁸, N. Herrmann¹⁸, L. Holub¹³, Y. Hong²⁷, S. Horvat⁶⁰, B. Huang¹¹, H. Z. Huang⁸, S. L. Huang⁴⁹, T. Huang³³, X. Huang⁵³, T. J. Humanic³⁵, P. Huo⁴⁹, G. Igo⁸, W. W. Jacobs²¹, A. Jentsch⁵², J. Jia^{5,49}, K. Jiang⁴⁵, S. Jowzaee⁵⁹, X. Ju⁴⁵, E. G. Judd⁶, S. Kabana²⁵, S. Kagamaster²⁸, D. Kalinkin²¹, K. Kang⁵³, D. Kapukchyan⁹, K. Kauder⁵, H. W. Ke⁵, D. Keane²⁵, A. Kechechyan²⁴, M. Kelsey²⁷, Y. V. Khyzhniak³¹, D. P. Kikoa⁵⁸, C. Kim⁹, T. A. Kinghorn⁷, I. Kisiel¹⁶, A. Kisiel⁵⁸, M. Kocan¹³, L. Kochenda³¹, L. K. Kosarzewski¹³, L. Kramarik¹³, P. Kravtsov³¹, K. Krueger⁴, N. Kulathunga Mudiyanselage¹⁹, L. Kumar³⁷, R. Kunawalkam Elayavalli⁵⁹, J. H. Kwasizur²¹, R. Lacey⁴⁹, J. M. Landgraf⁵, J. Lauret⁵, A. Lebedev⁵, R. Lednický²⁴, J. H. Lee⁵, C. Li⁴⁵, W. Li⁴⁷, W. Li⁴², X. Li⁴⁵, Y. Li⁵³, Y. Liang²⁵, R. Lisenik¹³, T. Lin⁵¹, A. Lipiec⁵⁸, M. A. Lisa³⁵, F. Liu¹⁰, H. Liu²¹, P. Liu⁴⁹, P. Liu⁴⁷, T. Liu⁶⁰, X. Liu³⁵, Y. Liu⁵¹, Z. Liu⁴⁵, T. Ljubicic⁵, W. J. Llope⁵⁹, M. Lomnitz²⁷, R. S. Longacre⁵, S. Luo¹¹, X. Luo¹⁰, G. L. Ma⁴⁷, L. Ma¹⁷, R. Ma⁵, Y. G. Ma⁴⁷, N. Magdy¹¹, R. Majka⁶⁰, D. Mallick³², S. Margetis²⁵, C. Markert⁵², H. S. Matis²⁷, O. Matonoha¹³, J. A. Mazer⁴³, K. Meehan⁷, J. C. Mei⁴⁶, N. G. Minaev³⁹, S. Mioduszewski⁵¹, D. Mishra³², B. Mohanty³², M. M. Mondal²², I. Mooney⁵⁹, Z. Moravcova¹³, D. A. Morozov³⁹, Md. Nasim⁸, K. Nayak¹⁰, J. M. Nelson⁶, D. B. Nemes⁶⁰, M. Nie⁴⁶, G. Nigmatkulov³¹, T. Niida⁵⁹, L. V. Nogach³⁹, T. Nonaka¹⁰, G. Odyniec²⁷, A. Ogawa⁵, K. Oh⁴¹, S. Oh⁶⁰, V. A. Okorokov³¹, B. S. Page⁵, R. Pak⁵, Y. Panebratsev²⁴, B. Pawlik³⁶, D. Pawlowska⁵⁸, H. Pei¹⁰, C. Perkins⁶, R. L. Pinter¹⁵, J. Pluta⁵⁸, J. Porter²⁷, M. Posik⁵⁰, N. K. Pruthi³⁷, M. Przybycien², J. Putschke⁵⁹, A. Quintero⁵⁰, S. K. Radhakrishnan²⁷, S. Ramachandran²⁶, R. L. Ray⁵², R. Reed²⁸, H. G. Ritter²⁷, J. B. Roberts⁴², O. V. Rogachevskiy²⁴, J. L. Romero⁷, L. Ruan⁵, J. Rusnak³⁴, O. Rusnakova¹³, N. R. Sahoo⁵¹, P. K. Sahu²², S. Salur⁴³, J. Sandweiss⁶⁰, J. Schambach⁵², W. B. Schmidke⁵, N. Schmitz²⁹, B. R. Schweid⁴⁹, F. Seck¹⁴, J. Seger¹², M. Sergeeva⁸, R. Seto⁹, P. Seyboth²⁹, N. Shah⁴⁷, E. Shahaliev²⁴, P. V. Shanmuganathan²⁸, M. Shao⁴⁵, F. Shen⁴⁶, W. Q. Shen⁴⁷, S. S. Shi¹⁰, Q. Y. Shou⁴⁷, E. P. Sichtermann²⁷, S. Siejka⁵⁸, R. Sikora², M. Simko³⁴, J. Singh³⁷, S. Singha²⁵, D. Smirnov⁵, N. Smirnov⁶⁰, W. Solyst²¹, P. Sorensen⁵, H. M. Spinka⁴, B. Srivastava⁴⁰, T. D. S. Stanislaus⁵⁶, M. Stefaniak⁵⁸, D. J. Stewart⁶⁰, M. Strikhanov³¹, B. Stringfellow⁴⁰, A. A. P. Suade⁴⁴, T. Sugiura⁵⁴, M. Sumbera³⁴, B. Summa³⁸, X. M. Sun¹⁰, Y. Sun⁴⁵, Y. Sun²⁰, B. Surrow⁵⁰, D. N. Svirida³, P. Szymanski⁵⁸, A. H. Tang⁵, Z. Tang⁴⁵, A. Taranenko³¹, T. Tarnowsky³⁰, J. H. Thomas²⁷, A. R. Timmins¹⁹, D. Tlusty¹², T. Todoroki⁵, M. Tokarev²⁴, C. A. Tomkiew²⁸, S. Trentalange⁸, R. E. Tribble⁵¹, P. Tribedy⁵, S. K. Tripathy²², O. D. Tsai⁸, B. Tu¹⁰, T. Ullrich⁵, D. G. Underwood⁴, I. Upsal^{46,5}, G. Van Buren⁵, J. Vanek³⁴, A. N. Vasiliev³⁹, I. Vassiliev¹⁶, F. Videbæk⁵, S. Vokal²⁴, S. A. Voloshin⁵⁹, F. Wang⁴⁰, G. Wang⁸, P. Wang⁴⁵, Y. Wang¹⁰, Y. Wang⁵³, J. C. Webb⁵, L. Wen⁸, G. D. Westfall³⁰, H. Wieman²⁷, S. W. Wissink²¹, R. Witt⁵⁵, Y. Wu²⁵, Z. G. Xiao⁵³, G. Xie¹¹, W. Xie⁴⁰, H. Xu²⁰, N. Xu²⁷, Q. H. Xu⁴⁶, Y. F. Xu⁴⁷, Z. Xu⁵, C. Yang⁴⁶, Q. Yang⁴⁶, S. Yang⁵, Y. Yang³³, Z. Ye⁴², Z. Ye¹¹, L. Yi⁴⁶, K. Yip⁵, I.-K. Yoo⁴¹, H. Zbroszczyk⁵⁸, W. Zha⁴⁵, D. Zhang¹⁰, L. Zhang¹⁰, S. Zhang⁴⁵, S. Zhang⁴⁷, X. P. Zhang⁵³, Y. Zhang⁴⁵, Z. Zhang⁴⁷, J. Zhao⁴⁰, C. Zhong⁴⁷, C. Zhou⁴⁷, X. Zhu⁵³, Z. Zhu⁴⁶, M. Zurek²⁷, M. Zyzak¹⁶

¹Abilene Christian University, Abilene, Texas 79699

²AGH University of Science and Technology, FPACS, Cracow 30-059, Poland

³Alikhanov Institute for Theoretical and Experimental Physics, Moscow 117218, Russia

⁴Argonne National Laboratory, Argonne, Illinois 60439

⁵Brookhaven National Laboratory, Upton, New York 11973

⁶University of California, Berkeley, California 94720

⁷University of California, Davis, California 95616

⁸University of California, Los Angeles, California 90095

⁹University of California, Riverside, California 92521

¹⁰Central China Normal University, Wuhan, Hubei 430079

¹¹University of Illinois at Chicago, Chicago, Illinois 60607

¹²Creighton University, Omaha, Nebraska 68178

¹³Czech Technical University in Prague, FNSPE, Prague 115 19, Czech Republic

- ¹⁴Technische Universität Darmstadt, Darmstadt 64289, Germany
¹⁵Eötvös Loránd University, Budapest, Hungary H-1117
¹⁶Frankfurt Institute for Advanced Studies FIAS, Frankfurt 60438, Germany
¹⁷Fudan University, Shanghai, 200433
¹⁸University of Heidelberg, Heidelberg 69120, Germany
¹⁹University of Houston, Houston, Texas 77204
²⁰Huzhou University, Huzhou, Zhejiang 313000
²¹Indiana University, Bloomington, Indiana 47408
²²Institute of Physics, Bhubaneswar 751005, India
²³University of Jammu, Jammu 180001, India
²⁴Joint Institute for Nuclear Research, Dubna 141 980, Russia
²⁵Kent State University, Kent, Ohio 44242
²⁶University of Kentucky, Lexington, Kentucky 40506-0055
²⁷Lawrence Berkeley National Laboratory, Berkeley, California 94720
²⁸Lehigh University, Bethlehem, Pennsylvania 18015
²⁹Max-Planck-Institut für Physik, Munich 80805, Germany
³⁰Michigan State University, East Lansing, Michigan 48824
³¹National Research Nuclear University MEPhI, Moscow 115409, Russia
³²National Institute of Science Education and Research, HBNI, Jatni 752050, India
³³National Cheng Kung University, Tainan 70101
³⁴Nuclear Physics Institute of the CAS, Rez 250 68, Czech Republic
³⁵Ohio State University, Columbus, Ohio 43210
³⁶Institute of Nuclear Physics PAN, Cracow 31-342, Poland
³⁷Panjab University, Chandigarh 160014, India
³⁸Pennsylvania State University, University Park, Pennsylvania 16802
³⁹NRC "Kurchatov Institute", Institute of High Energy Physics, Protvino 142281, Russia
⁴⁰Purdue University, West Lafayette, Indiana 47907
⁴¹Pusan National University, Pusan 46241, Korea
⁴²Rice University, Houston, Texas 77251
⁴³Rutgers University, Piscataway, New Jersey 08854
⁴⁴Universidade de São Paulo, São Paulo, Brazil 05314-970
⁴⁵University of Science and Technology of China, Hefei, Anhui 230026
⁴⁶Shandong University, Qingdao, Shandong 266237
⁴⁷Shanghai Institute of Applied Physics, Chinese Academy of Sciences, Shanghai 201800
⁴⁸Southern Connecticut State University, New Haven, Connecticut 06515
⁴⁹State University of New York, Stony Brook, New York 11794
⁵⁰Temple University, Philadelphia, Pennsylvania 19122
⁵¹Texas A&M University, College Station, Texas 77843
⁵²University of Texas, Austin, Texas 78712
⁵³Tsinghua University, Beijing 100084
⁵⁴University of Tsukuba, Tsukuba, Ibaraki 305-8571, Japan
⁵⁵United States Naval Academy, Annapolis, Maryland 21402
⁵⁶Valparaiso University, Valparaiso, Indiana 46383
⁵⁷Variable Energy Cyclotron Centre, Kolkata 700064, India
⁵⁸Warsaw University of Technology, Warsaw 00-661, Poland
⁵⁹Wayne State University, Detroit, Michigan 48201
⁶⁰Yale University, New Haven, Connecticut 06520

Methods

This methods section describes the details of recalibration for the previous B_Λ measurements. The Λ binding energy for the 2-body and 3-body decays of the hypertriton are defined as⁴⁰

$$B_\Lambda^{\text{2-body}} = m_\Lambda + m_d - m_{^3\text{He}} - m_{\pi^-} - Q = Q_0 - Q \quad (2)$$

$$B_\Lambda^{\text{3-body}} = m_\Lambda + m_d - m_d - m_p - m_{\pi^-} - Q' = Q'_0 - Q' \quad (3)$$

where Q and Q' are the total kinetic energies released in these hypertriton decays, and Q_0 and Q'_0 are the constants defined by the equations above. In the studies being updated here, Q (Q') was determined from the length of decay daughter tracks, based on the range versus energy relationship for that charged particle species in nuclear emulsion or in a He bubble chamber. The published B_Λ values were calculated using the contemporaneous mass values for Λ , π^- , p , d , ^3He , as reproduced in Table 1, which can be seen to differ from the best current numbers. Q_0 (Q'_0) has been recalculated using current numbers and the B_Λ values for past emulsion and bubble chamber studies are thus recalibrated in this letter.

Table 1 | Assumed masses in past and present determinations of hypertriton binding energy B_Λ . All masses are in units of MeV/c^2 .

Measurements	Λ mass	π^- mass	p mass	d mass	^3He mass
Gajewski <i>et al.</i> (1967) ³¹	1115.44 ³²	139.59 ⁴¹	938.26 ⁴¹	1875.50 ^{40,45,46}	2808.22 ^{40,45,46}
Bohm <i>et al.</i> (1968) ³²	1115.57 ³²	139.58 ⁴²	938.26 ⁴²	1875.50 ^{40,45,46}	2808.22 ^{40,45,46}
Keyes <i>et al.</i> (1970) ³³	1115.67 ³³	139.58 ⁴³	938.26 ⁴³	1875.58 ³³	2808.22 ^{40,45,46}
Bohm <i>et al.</i> (1973) ⁴	1115.57 ⁴	139.58 ⁴⁴	938.26 ⁴⁴	1875.50 ^{40,45,46}	2808.22 ^{40,45,46}
Present study	1115.68 ¹⁸	139.57 ¹⁸	938.27 ¹⁸	1875.61 ³⁰	2808.39 ³⁰

Table 2 | The previous measurements of B_Λ for hypertriton and its corresponding recalibration results. B_Λ is in units of MeV. The uncertainties are the reported statistical uncertainties.

Measurements	Original		Recalibrated	
	B_Λ	Combined B_Λ	B_Λ	Combined B_Λ
Gajewski <i>et al.</i> (1967) ³¹	0.13 ± 0.15 (2-body)	0.20 ± 0.12	0.33 ± 0.15 (2-body)	0.41 ± 0.12
	0.33 ± 0.21 (3-body)		0.58 ± 0.21 (3-body)	
Bohm <i>et al.</i> (1968) ³²	0.05 ± 0.08 (2-body)	0.01 ± 0.07	0.11 ± 0.08 (2-body)	0.08 ± 0.07
	-0.11 ± 0.13 (3-body)		0.00 ± 0.13 (3-body)	
Keyes <i>et al.</i> (1970) ³³	0.25 ± 0.31 (2-body)	-0.07 ± 0.27	0.13 ± 0.31 (2-body)	-0.16 ± 0.27
	-0.74 ± 0.43 (3-body)		-0.73 ± 0.43 (3-body)	
Bohm <i>et al.</i> (1973) ⁴	0.06 ± 0.11 (2-body)	0.15 ± 0.08	0.12 ± 0.11 (2-body)	0.23 ± 0.08
	0.23 ± 0.11 (3-body)		0.34 ± 0.11 (3-body)	

References

- [40] Slater, W. E. A systematic study of hyperfragments produced by 4.5 GeV π^- in nuclear emulsion. *Nuovo Cimento* **10** (Suppl 1), 1-40 (1958).
- [41] Mayeur, C. *et al.* A determination of the B_Λ values of light hypernuclei. *Nuovo Cimento* **43**, 180-192 (1966).
- [42] Rosenfeld, A. H. *et al.* Data on particles and resonant states. *Rev. Mod. Phys.* **39**, 1-51 (1967).
- [43] Barash-Schmidt, N. *et al.* (Particle Data Group) Review of particle properties. *Rev. Mod. Phys.* **41**, 109-192 (1969).
- [44] Barash-Schmidt, N. *et al.* (Particle Data Group) Tables of particle properties. (1972) <http://pdg.lbl.gov/rpp-archive/files/cm-p00040028.pdf>
- [45] Everling, F., Konig, L. A., Mattauch, J. H. E. & Wapstra, A. H. Relative nuclidic masses. *Nucl. Phys.* **18**, 529-569 (1960).
- [46] Wapstra, A. H. Isotopic masses I. $A < 34$. *Physica* **21**, 367-384 (1954).